



**UNIVERSITY OF LEEDS**

This is a repository copy of *X-ray system simulation software tools for radiology and radiography education*.

White Rose Research Online URL for this paper:  
<http://eprints.whiterose.ac.uk/125794/>

Version: Accepted Version

---

**Article:**

Kengyelics, SM, Treadgold, LA [orcid.org/0000-0001-5493-4165](https://orcid.org/0000-0001-5493-4165) and Davies, AG (2018)  
*X-ray system simulation software tools for radiology and radiography education*.  
*Computers in Biology and Medicine*, 93. pp. 175-183. ISSN 0010-4825

<https://doi.org/10.1016/j.compbiomed.2017.12.005>

---

(c) 2017, Elsevier Ltd. This manuscript version is made available under the CC BY-NC-ND 4.0 license <https://creativecommons.org/licenses/by-nc-nd/4.0/>

**Reuse**

This article is distributed under the terms of the Creative Commons Attribution-NonCommercial-NoDerivs (CC BY-NC-ND) licence. This licence only allows you to download this work and share it with others as long as you credit the authors, but you can't change the article in any way or use it commercially. More information and the full terms of the licence here: <https://creativecommons.org/licenses/>

**Takedown**

If you consider content in White Rose Research Online to be in breach of UK law, please notify us by emailing [eprints@whiterose.ac.uk](mailto:eprints@whiterose.ac.uk) including the URL of the record and the reason for the withdrawal request.



[eprints@whiterose.ac.uk](mailto:eprints@whiterose.ac.uk)  
<https://eprints.whiterose.ac.uk/>

# X-ray System Simulation Software Tools for Radiology and Radiography Education

Stephen M Kengyelics, Laura A Treadgold, Andrew G Davies

Specialist Science Education Department

Leeds Institute of Cardiovascular and Metabolic Medicine

School of Medicine

University of Leeds

Leeds, UK

Corresponding Author:

Andrew Davies

Tel: +44 113 343 8313

Email: [a.g.davies@leeds.ac.uk](mailto:a.g.davies@leeds.ac.uk)

## **Abstract**

**Objectives** To develop x-ray simulation software tools to support delivery of radiological science education for a range of learning environments and audiences including individual study, lectures, and tutorials.

**Methods** Two software tools were developed; one simulated x-ray production for a simple two dimensional radiographic system geometry comprising an x-ray source, beam filter, test object and detector. The other simulated the acquisition and display of two dimensional radiographic images of complex three dimensional objects using a ray casting algorithm through three dimensional mesh objects. Both tools were intended to be simple to use, produce results accurate enough to be useful for educational purposes, and have an acceptable simulation time on modest computer hardware. The radiographic factors and acquisition geometry could be altered in both tools via their graphical user interfaces. A comparison of radiographic contrast measurements of the simulators to a real system was performed.

**Results** The contrast output of the simulators had excellent agreement with measured results. The software simulators were deployed to 120 computers on campus.

**Conclusions** The software tools developed are easy-to-use, clearly demonstrate important x-ray physics and imaging principles, are accessible within a standard University setting and could be used to enhance the teaching of x-ray physics to undergraduate students.

**Advances in knowledge** Current approaches to teaching x-ray physics in radiological science lack immediacy when linking theory with practice. This

method of delivery allows students to engage with the subject in an experiential learning environment.

## 1 INTRODUCTION

A comprehensive understanding of x-ray physics is essential to a number of professional roles in healthcare including radiography, radiology, and medical physics. Therefore, its teaching forms an integral part of the training for a number of associated professional qualifications. Traditional teaching methods for delivering x-ray physics education have focussed on didactic lectures that may not be effective for a number of reasons depending on the student group. Some students have little relevant mathematics or physics education or have not engaged with this material for some time. For some student groups, interpreting and linking complex physical processes, which are often described mathematically, to real-world situations is often challenging and can lead to poor student engagement.

Demonstrating x-ray imaging physics through experimental measurements would be beneficial, but requires access to x-ray equipment which is not always available for teaching this subject, or is limited in relation to access and the number of students involved. This approach would also have radiation protection issues, requiring students to be closely monitored within a properly audited risk-assessment framework. This would clearly have an impact on the ability to deliver the teaching in this way, affecting the number of staff required, associated training, and running costs. It is often the case that work-based clinical placements support the delivery of clinical practice but not the underpinning theory, and are not always delivered in parallel, making it difficult for a student to form a clear link between theory and practice.

An alternative to direct experimentation is the use of computer simulators. Existing techniques for the simulation of x-ray imaging systems have focussed primarily on

Monte Carlo (MC) methods [1–13]. In general, these techniques are computationally expensive even when supported by graphical processing unit (GPU) acceleration [1–7] or when combined with deterministic calculations to speedup computation times [6,12,13]. Other deterministic methods [14–22] employ ray or pencil beam tracing techniques using computed tomography (CT) volumes [14–17] or meshes [18,20–22] to produce forward-projected radiographic 2D x-ray images. The majority of these MC, deterministic, or hybrid approaches are aimed at specialist applications such as x-ray system optimisation or 2D/3D image registration. These software packages often require specialist physics and computer programming knowledge to operate and interpret. Therefore, they are not well suited for general educational purposes. In addition, many of the techniques require GPU support which is not readily available on computers used by students for educational purposes. The few contributions aimed at educational applications are limited. In 2005 Fanti et al. [16] presented a simple x-ray simulation system based on pencil beam forward projections through a CT volume formed by stacking a number of slices formed by 256 pixels × 256 pixels × 1 mm wide that resulted in the final image. The image detector in this model had the same response as photographic film and not a modern digital detector. Dikshit et al [19] presented an online interactive simulation system for medical imaging education deployed using MALAB Web Server environment. However, only a single slice CT simulator and one dimension beam x-ray attenuation model was reported. To the best of our knowledge no further developments to either of the two preceding contributions were reported. A commercially available software, Shaderware, has been available since 2006, and has seen active development since then. To our knowledge its underlying algorithms have not been described in the literature, but appears to utilise forward projection of CT volumes for its imaging.

In this study we have developed two innovative software tools to simulate many practical aspects of x-ray production, image acquisition and display. Unlike general x-ray simulators, or those used for research purposes, these tools were specifically aimed at demonstrating key learning points through an interactive environment. As such they do not attempt to simulate every aspect of a real system, only those that require demonstrating within the teaching of x-ray physics to student groups new to the subject. It is also important that the simulation operates sufficiently quickly for interactive teaching purposes (whereas a research simulator may take considerably longer to compute results). A constrained feature design enabled the simulators to operate in real-time with relatively modest computer system requirements yet retain sufficient realism within the simulation to support learning. The tools are easy to implement and deploy on standard personal computers (PCs) and employ readily available anatomical mesh libraries and physics data files. As such the tools scale well with student numbers and represent a much more economical approach compared with commercially available alternatives, albeit with reduced features and complexity. Operating the tools do not require specialist programming skills and, due to the modular nature of the computer code, are easily updated and extended to incorporate additional features. The delivery of x-ray physics teaching through this innovative and accessible method will allow students to understand the theory and relationship with clinical practice thereby developing a deeper understanding of the subject. In summary, the developed software tools provide a novel learning environment that is easily deployable and does not require any special training or knowledge on the part of the student. Though sacrificing some realism, the tools clearly demonstrates key principles of x-ray production and imaging.

## 2 METHODS AND MATERIALS

We have developed two software packages based on our underlying simulation software. The first tool, EX-RayCalc, focussed on x-ray production physics, while the second, EX-RayImage, on simulating image capture and display of anatomically realistic structures. The software tools were developed and tested using MATLAB [23]. Each software tool provides a single window graphical user interface (GUI), and utilises a set of common simulation stages which are described below. The software tools may be deployed in a number of environments. Any computer supporting the MATLAB runtime environment, which are recent Microsoft Windows, Apple Mac and LINUX based computers with modest hardware (4 Gb RAM, i3 CPU or better), can run the software. The overall system design of the two software tools is shown in Figure 1. Referring to Figure 1, both tools share the same x-ray production simulation component. The output x-ray spectrum is calculated using user defined input parameters of x-ray tube voltage (kVp), x-ray tube current (mA), pulse duration (ms), and x-ray beam filtration. For EX-RayCalc the user can specify the thickness of a PMMA test phantom and the distance of the x-ray source from the entrance of the phantom and the detector plane. The tool calculates and displays the entrance surface dose (ESD), x-ray photon fluence, and the mean x-ray beam energy for both the entrance to the test phantom and at the detector plane. The input and output x-ray spectra are also calculated and displayed. EX-RayImage replaces the simple PMMA phantom of EX-RayCalc with anatomical mesh files to generate realistic looking radiographic images. The user can select a number of different meshes that can be rotated about X, Y and Z axes, and positioned between the x-ray source and detector. When the user initiates an x-ray exposure to generate a radiograph, a forward projection through the mesh is used to calculate a depth image at the

detector plane. The depth image represents the thickness of each material encountered by a ray traced from the x-ray source to the detector for each pixel of the detector array. Using the depth image, the input x-ray spectrum, and the calculated fractional absorption of the image detector, a digital image is generated. Added noise and image blur are applied, followed by a signal gain stage and digital level quantization. The user can select a number of optional image scaling schemes to apply to the resultant image.

## 2.1 X-ray production simulation

The x-ray tube was assumed to have a point source, 12 degrees anode angle, W anode target material, 0% waveform ripple, and 2 mm Al inherent filtration. X-ray spectra were calculated from published tables [24] for the stated conditions for 50–120 kVp, in 1.0 kVp increments according to Equation (1)

$$S_o(E) = S_i(E)e^{-\mu_m(E)\rho x} \quad (1)$$

Where  $S_i(E)$  and  $S_o(E)$  are the input and output x-ray spectra respectively, as functions of photon energy  $E$  expressed in electron volts,  $\mu_m(E)$  is the mass attenuation coefficient of the filtering material expressed in units  $\text{cm}^2/\text{g}$ ,  $\rho$  is the density in units of  $\text{g}/\text{cm}^3$  and  $x$  is the thickness of the filtration in cm. Mass attenuation and density values were obtained from published tables [25].  $S_o(E)$  is expressed as the number of photons/ $\text{mm}^2/\text{mAs}$  at a source-to-detector distance of 750 mm for each energy increment. The output spectra were stored in files for use by the software tool. An output x-ray spectrum was generated from one of the stored spectra using supplied parameters: x-ray tube voltage, current, exposure time, and the source to image-receptor distance (SID). The appropriate spectrum was selected

by kVp and adjusted to compensate for the product of mA and ms, and for the effect of the inverse square law. The spectrum could be further modified by the additional beam filtration, and where appropriate the object material, using available mass attenuation coefficients and material density values [25].

### **2.1.1 X-ray production validation**

**To validate the x-ray production simulator a series of measurements were performed using the experimental setup shown in**

Figure 2 using an Allura FD10 cardiac x-ray imaging system (Philips Healthcare, NL). The imaging system was modified by the manufacturer to allow image data capture prior to the standard digital image processing enhancement algorithms used for clinical images. The x-ray detector employed is a flat-panel image detector (FPID) of an indirect type, whereby a thallium-doped cesium-iodide (CsI:TI) phosphor detection layer converts incident x-ray photons to visible light photons. The light photons are detected by an amorphous silicon (a:Si) photodiode, thin-film transistor (TFT), sensor array. Each element containing a photodiode converts the detected light photons to a proportional electrical charge that is stored locally and subsequently read out, amplified and converted to digital data. Image sequences were generated for a plastic test phantom comprising slabs of PMMA measuring 25 cm × 25 cm × 2.5 cm, for a total phantom thickness of 15-30 cm in increments of 2.5 cm at a frame rate of 30 frames per second. The PMMA slabs were supported above the couch (patient table) by 40 mm thick spacers, allowing the placement of test details directly on to the top surface of the couch. The x-ray tube voltage and current were recorded for all measurements. The automatic dose rate control of the imaging

system is designed to maintain a specified average signal level from the detector by adjusting system parameters in response to changes of x-ray beam attenuation resulting, for example, in variations of patient thickness or image projection. A tin contrast detail measuring 10 mm × 10 mm × 0.3 mm was placed on the top surface of the couch, which is 40 mm (the width of the PMMA supporting spacers) underneath the entrance surface of the PMMA phantom where the x-ray beam enters. Measured contrast  $C$  was calculated from the final image according to:

$$C = \frac{s - b}{b}$$

Where  $s$  is the mean digital value of pixel values due to the detail and  $b$  is the mean of pixel values in the background of the detail. X-ray attenuation predictions according to the simulator model for the contrast of the Sn detail were performed in the absence of scatter for the experimental conditions recorded and using the parameters listed in Table 1. The x-ray absorption of the CsI detection layer was estimated using published tables [24,25].

Anode material	W
Anode angle (Degrees)	9.0
% Ripple	0
Inherent filtration	0.2 mm Al
Additional filtration	0.4 mm Cu
CsI:TI effective thickness	0.480 mm
Sn detail thickness	0.3 mm

**Table 1. X-ray production parameters**

Measured contrast is subject to degradation by x-ray scatter and needs to be accounted for in order to compare the predicted contrast values calculated by the simulator model, which does not account for scatter, with those obtained experimentally. Measured contrast values are reduced by scatter degradation factor defined by Equation (2)

$$SDF = \frac{1}{1+S/P}$$
(2)

Where  $S/P$  is the scatter-to-primary ratio (SPR). An estimate of the SPR at the entrance to the image detector was calculated using a series of three lead (Pb) circular disks, 3 mm thick, with diameters 2, 5, and 7 mm, placed on the top surface of the couch and laterally spaced within 1 cm of each other and approximately 2.5 cm from the center of the image field, as shown in 3.1. Image sequences were temporally averaged over all frames to reduce image noise. The average digital values calculated at the center of each disk as a function of the measurement aperture were extrapolated to zero diameter yielding an estimate of scatter. Using these values and average digital values in the background of the disks the SPR was calculated. The SDF was then calculated according to Equation (2), and applied to the predicted contrast values. The resulting values were then compared to the measured results. This allows the contrast values predicted by the simulator to be compared to the measured contrast values over the range of x-ray exposure factors considered.

## 2.2 X-ray image formation

Anatomical and phantom structures in the simulation were represented by triangular-based mesh files and were used to generate simulated radiographic 2D projection

images. Multiple meshes objects may be employed to represent complex anatomy and can be rotated in space and translated between x-ray source and detector. Any suitable mesh file can be used, whether representing human anatomy or other shapes. We used available anatomy mesh files from an online database:

BodyParts3D, Copyright 2008, Database Center for Life Science licensed by CC Display - Share Alike 2.1 Japan. See also Mitsuhashi et al. [26]

Projected distances of ray intersections through complex 3D meshes were calculated to determine the total distance traversed of each material encountered along individual rays. We adapted and extended a method due to Freud et al. [21] to account for the attenuation of multiple meshes representing the same, or different materials, that may be arranged in a number of configurations. The core method used by Freud is identical to our method and therefore it is expected to have equivalent performance in terms of accuracy.

### **2.2.1 Algorithm description**

A detector is represented by a square array of points orientated at the center of square pixel elements. The simulation proceeds by tracing the path of rays represented by straight lines between the point source to the detector pixel centers. Individual mesh objects are defined by triangular faces defined from a list of vertices. The following assumptions are made. A ray entering a mesh will leave the mesh before reaching the detector plane. A single mesh objects is comprised of a uniform material of known composition and density. Meshes can fully enclose other meshes. Only meshes representing the same material can intersect. Currently, only primary radiation is considered.

### 2.2.2 Overview of algorithm

- A. Project the vertices of each mesh face onto the detector plane.
- B. Determine which pixels of the detector lay inside a bounding rectangle defined by the maximum and minimum values of the three vertices in both X and Y directions.
- C. For those points inside the bounding rectangle determine if the point was inside the original triangle and if so calculate the point of intersection.
- D. For each source to pixel ray determine the path length for each material represented by any number of meshes by accumulating the distances travelled in each material.
- E. Determine the attenuation of the ray for all of the materials along the path length for the radiographic factors requested.

### 2.2.3 Step A

To determine the total distance traversed by a ray emanating from the point x-ray source and terminating at the center of a pixel element through an individual mesh requires calculation of the intersection points of entry and exit with the mesh surface. This would generally require considering each ray against each mesh face. Even for a moderately sized detector array and mesh, the number of calculations becomes prohibitive if anywhere near real-time operation is required. However, the number of calculations can be greatly reduced by only considering rays that are within a boundary defined by a mesh face projected on to the 2D detector plane as will be described.

The position of point  $P$  on a straight line can be described by the parametric equation:

$$P = L_0 + sL$$

(3)

Where  $s$  is a scalar,  $L_0$  is a point on the line, and  $L$  is a vector in the direction of the line.

The vector  $L$  can be determined given any two points on the line by:

$$L = L_1 - L_0$$

(4)

Where  $L_1$  is a point on the line in addition to  $L_0$ .

The position of a point  $P$  on a plane, as shown in

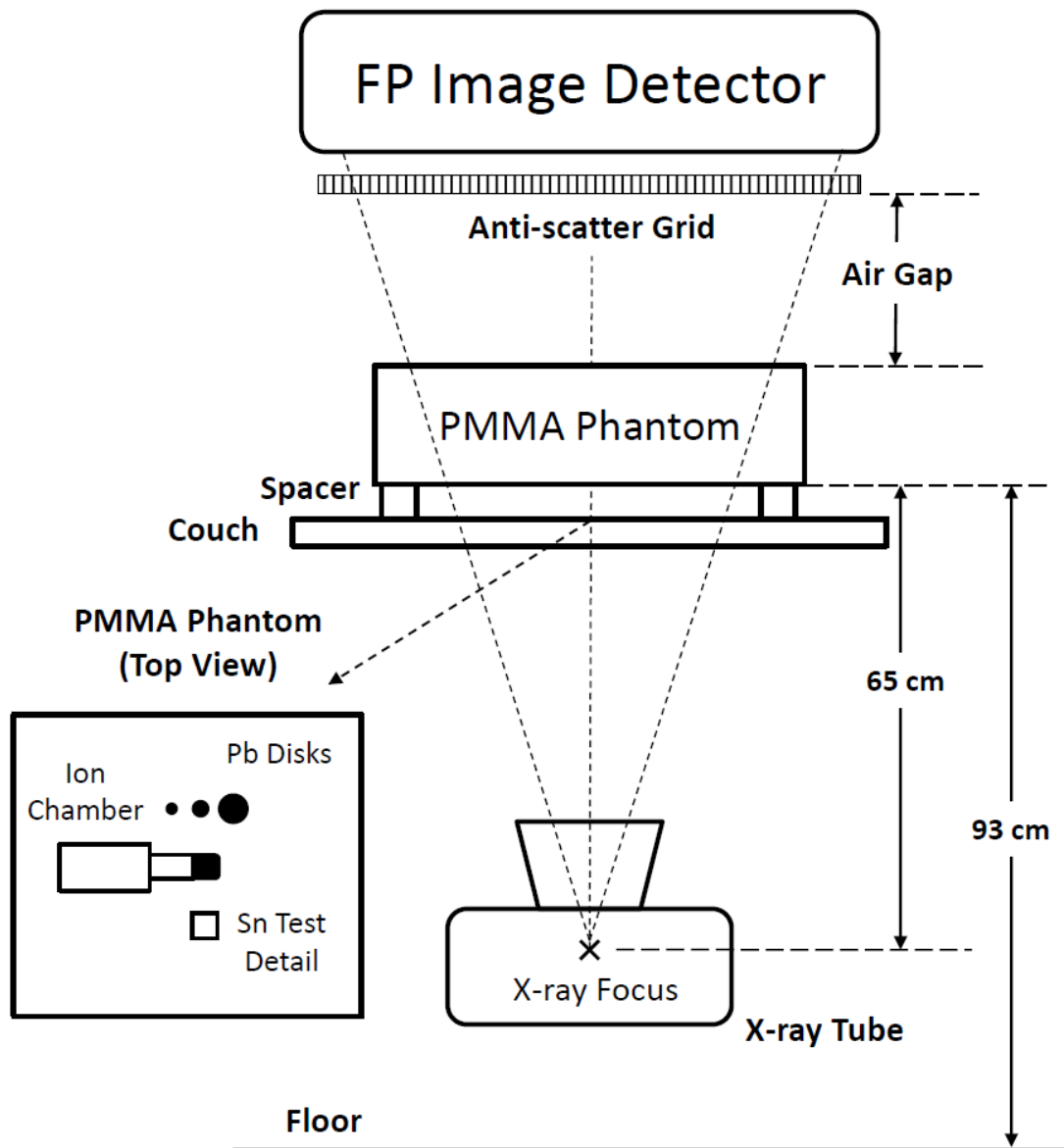


**Figure 3**, satisfies the relationship

$$(P - P_0) \cdot \mathbf{n} = 0 \tag{5}$$

Where  $P_0$  is a point on the plane,  $\mathbf{n}$  is a vector normal to the plane and the scalar product is denoted by the dot.

To determine the value of the scalar where the line intersects the plane, Equation (3) is substituted into Equation (5). Solving for  $s$  yields

$$s = \frac{(P_0 - L_0) \cdot \mathbf{n}}{\mathbf{L} \cdot \mathbf{n}} \tag{4}$$

If  $\mathbf{L} \cdot \mathbf{n} = 0$  the line is parallel to the plane, either in or out of the plane. If  $\mathbf{L} \cdot \mathbf{n} \neq 0$  then there is a single point of intersection that can be calculated from Equation (3).

#### **2.2.4 Step B**

Using the above, each vertex from each face of a mesh can be forward projected from the direction of the point x-ray source onto the XY plane of the detector as illustrated in Figure 4. Only pixel elements falling inside the bounding box are then used to test for ray intersections with the face.

#### **2.2.5 Step C**

We used an algorithm due to Möller and Trumbore [27] to test if the rays intersect with the plane that the mesh face is on and if so whether or not it inside the triangle formed by the vertices. If the ray falls inside the triangle then the point of intersection is returned and the distance of the intersection from the source is calculated. Freud et al. [21] determined which pixels are inside the triangle using a classical polygon

filling operation whereas we only consider those bound by a rectangle for convenience and then perform a test to determine for intersection using the algorithm of Möller and Trumbore [27]. The use of rectangular bounding results in more rays being evaluated for collision per triangular facet compared with the method of Freud et al., but from a practical point-of-view the time overhead was not prohibitive for the application. This operation is repeated for all the faces of all the meshes in a scene. This generates a list of intersection distances from the x-ray source for each ray and the associated mesh for which the intersection took place.

### **2.2.6 Step D**

This list is then sorted with respect to the intersection distance, smallest to largest. The sorted list now represents the intersection distances in the order the projected ray encounter the meshes as it transversed from the source to the detector. The distance that a particular ray transverses through a given mesh is then calculated by considering the intersection distances and which meshes were entered or exited. The algorithm developed accounts for a number of general scenarios that are illustrated for convenience in 2D in

Figure 5 and any combination of these cases.

Figure 5(a) illustrates multiple meshes representing the same material that overlay one another,

Figure 5(b) shows the same geometry, but each mesh representing a different material.

Figure 5(c) shows the case where a mesh of the same material intersects another mesh. This case occurs for a large number of meshes in the BodyParts3D database used in this project. The ill-posed case where two meshes, intended to represent different materials, intersect one another, in that they are enmeshed with each other, is not considered as it does not occur in the mesh database used to the best of our current knowledge. However, it is possible that this case may occur in other databases and result in the boundary of each material being indeterminate in the intersecting region.

Figure 5(d) illustrates the last case where complete enclosure of meshes inside other meshes.

Only ray intersection distances for a mesh are known, not whether a ray is entering a mesh or leaving it. To calculate the distance a ray traverses within each mesh a stack data structure is used keep track of where the ray enters and leaves a specific mesh. Each mesh has its own identifying mesh index and is associated with a particular material. When a ray intersects the first mesh the mesh index is pushed onto the stack. At the next intersection if the mesh index is the same then the stack is popped. If it is different then it is pushed onto the stack. The values of mesh index values entering or leaving the stack are recorded for each intersection point. From this record the total distance traversed by each ray for each mesh encountered is calculated.

### **2.2.7 Step E**

Finally, the attenuation of the ray for all of the materials along the path length for the radiographic factors requested is calculated using the spectrum calculated in section 2.1.

## **2.3 X-ray detection**

X-ray detection is simulated to reflect the processes in an indirect flat-panel x-ray detector. The number of photons absorbed in the CsI scintillator layer per pixel is calculated by summing the photon count in each ray from Step E, and correcting for the specified pixel area. Poisson distributed random noise added to each pixel value. A low pass filter is applied to the resultant image simulating unsharpness in the x-ray detector, followed by a signal gain (amplification), and the signal quantised

representing digitisation. The user could control the system gain, pixel size, and scintillator thickness.

## **2.4 Image display**

The image can be displayed either as the unprocessed detector pixel intensities, or following processing involving the following stages:

- Normalisation of the mean pixel value to a specified pixel intensity (optional)
- Range compression via a logarithmic pixel intensity transformation (optional)
- Image inversion allowing “white bone” display (optional)
- Window and level settings that could be interactively varied by the user or automatically calculated to auto-range the display.

Interactive tools allowed the user to measure pixel values, and perform basic intensity profile plots on acquired images.

## **2.5 Computational performance**

The software performance was assessed on a computer typical of those used in campus clusters at our University, specifically a Stone desktop PC (Stone Group PLC, Stafford, UK with an Intel Core i5-4570 processor(Intel Corporation, Santa Clara, CA). The PC was purchased in 2014. Computation times were tested with a number of different mesh structures and also the impact of altering the number of pixels was assessed. In all cases three simulated images were created with the time to compute the image and display the results calculated using MATLAB’s tic and toc functions, and the average time calculated.

### 3 RESULTS

#### 3.1 X-ray production simulation tool: EX-RayCalc

EX-Raycalc was designed to support the understanding of x-ray production (such as energy spectra), basic dosimetry, and attenuation. A simplified two dimensional geometry is presented with a vertical x-ray tube irradiating a single rectangular object. The user adjusts the kVp, mA, ms and SID by moving the sliders or entering the values directly in the associated text boxes. The object thickness and added filter thickness are selected via the drop down menus. Calculated values of entrance surface dose (ESD), photon fluence and mean x-ray beam energy are displayed in the measurements table for at both the object entrance surface and detector entrance surface. X-ray spectra are displayed and the unfiltered input spectrum, filtered input spectrum and the spectrum calculated at the detector entrance can be displayed independently or together. The x-ray tube position changes on the geometry axes when the SID changes, as does the size of the object when another object thickness is selected. Linear attenuation coefficients for both the applied filter and the object are displayed in the Filter Attenuation axes as a function of energy. The display updates in real-time in response to any change in the input parameters. The complete user interface for EX-RayCalc software tool is shown in

Figure 6.

### **3.1.1 X-ray production validation**

Figure 7 shows predicted and measured contrast values for the experimental conditions investigated. Measured scatter degradation factors were applied to the predicted contrast excluding scatter, calculated using the computational model, to yield predicted contrast values that include the effects of scatter. These show good agreement with the experimentally measured values across a wide range of kVp and PMMA values. Measured contrast values  $C_m$  are related to predicted values including scatter  $C_s$  by  $C_m = 0.99C_s + 0.01$ ,  $R^2 = 0.99$ .

### **3.2 X-ray image acquisition simulation and display tool: EX-**

#### **RayImage**

EX-RayImage models a 3D geometry represented with the point x-ray source, the object(s) to be imaged, and a detector in the XY plane with  $Z=0$ . A close up of the object to be imaged is also presented. The user may rotate objects around a common pre-defined center about either the X, Y, or Z-axis, and also, translate them between source and the detector along the Z axis. X-ray shutters can be positioned in either of the X or Y directions. A preview silhouette of the outline of the objects is displayed in the Plan View and the System Geometry view in the detector plane. After positioning the object and selecting the required radiographic factors, the user produces a simulated radiograph by clicking the expose button. The final image is displayed in the Output Image view. The main window of the user interface for EX-RayImage is shown in

Figure 8. The display and detector settings are altered in dialogue windows (not shown).

An example of a number of images produced from a) vertebra b) hand c) knee meshes are shown in

Figure 9.

Figure 10 shows an example of two simulated radiographic images generated using different factors. The first image is generated using 50 kVp and 1 mAs. The second image is generated at 120 kVp and 40 mAs. The first image clearly contains more noise and exhibits higher contrast than the second as would be expected. The first image has greater contrast than the second as a result of using a lower kVp x-ray beam. This results in a higher proportion of photoelectric absorption for bone in comparison to the high kVp case. However, the low kVp image is formed with 40 times lower mAs that results in excessive quantum noise in the resultant image. Increasing this value in the high kVp image results in a less noisy image.

### 3.3 Computational Performance

EX-RayCalc updated in real time on all computers on campus, with the output updating with no perceptible lag between altering a parameter and the outputs being displayed. The computational performance of EX-RayImage generating and displaying a 500 x 500 pixel image of the meshes used in Figures 9 and 10 is summarised in Table 2. Overall the average computation time was 7.5 s. Using the vertebra mesh it took 2.13, 4.92 and 16.09 s to compute an image with 250x250, 500x500 and 1000x1000 pixels respectively.

Mesh	N vertices	N faces	Average computation time (s)
Vertebra	2115	3892	4.92
Elbow	5290	3121	4.72
Hand & wrist	9722	6194	5.20

Pelvis	17321	31490	10.15
--------	-------	-------	-------

Table 2: Times to compute a 500 x 500 image on a desktop computer.

#### 4 DISCUSSION

The use of MATLAB, whilst offering us rapid application development, did have its drawbacks. The graphical user interface components are dated in appearance and are limited in functionality by modern standards. The requirement for the MATLAB runtime also adds a considerable installation overhead to the software package, and the dependency could introduce support issues, and because of this we did not distribute the stand alone application directly to students. Developing future versions as a web application, with no local installation, and calculations performed by a remote server, would overcome these issues.

The simulators offer a number of advantages over the use of real equipment. Any number of scenarios can be repeated without the use of ionizing radiation or the use of specialist equipment, giving immediate results and student feedback, and yielding sufficiently realistic results to support the learning objectives. The software can be deployed on multiple computers to service need of many students and used in multiple situations and at different learning levels such as self-learning, tutorial-led or lecture demonstrations. The interactive tools allows students to change factors that are not always possible on modern radiographic systems e.g. independent control of mA and ms, and beam filtration. The use of mesh files allows 3D printing of anatomy to further aid the student in the interpretation of flat 2D projection images.

As with any simulated environment there are a number of limitations when compared to the real practical situation. For example, when performing the measurements using the x-ray calculator scattered radiation is not currently considered and,

therefore, the measurements made are not exactly that which would be found in practice. In such circumstances it is important that these aspects should be noted in supporting lectures, or workbooks, and the impact discussed. The modelling of structures using meshes where the interior is assumed to be a homogenous material is also unrealistic. While surprisingly convincing in many cases, the simulated images do not possess the subtle details found in real radiographic images, especially for bony structures where the distribution of compact bone and cancellous bone is not represented. The use of more complex meshes, or more complex attenuation profile calculations could allow for non-uniform objects to be more realistically represented. The use of meshes does offer the potential to implement a deformable set of structures, and allow structures to move with respect to one another, for instance simulating different joint articulations. The software tools and mesh files that they utilise, are currently being developed further, and once a more stable state, it is our intention to release the software as open source. In the meantime, access to the tools can be obtained by contacting the authors.

The x-ray detector simulated was only of one type- i.e. indirect solid state detector. This is probably the most common detector design in use currently, and alternatives (such as computed radiography or direct solid state detectors) would not have yielded significantly different results. Given the lack of scatter, focal spot unsharpness, and non-quantum noise sources (such as electronic noise) both the noise and modulation transfer functions of the simulated system would not precisely match any real device, and hence the simulated images would not be a precise match for a real system. The system was internally consistent (so for example changes in pixel size would affect the resultant pixel intensity as expected), and as such could still be used to illustrate a wide educational points. As the simulator is

further developed, we aim to match more closely the output of specific detector systems. The image processing stages that the simulator implements are simplistic by real system standards- there is no sophisticated computer enhancement as is common in modern radiography systems, but normalisation, automatic range and image inversion were selectable.

In terms of the learning points that the simulator was designed to be used for a range of educators at the University gave input to the project, including members with a medical physics and radiography teams. Consideration was given to the learning objectives that we would prioritise, which derived the feature set of the simulators, and their user interfaces. This education input resulted in the production of two separate applications which could be used in different parts of teaching, and focussed on both having user interfaces designed to be used with minimum guidance to users. The team also made pragmatic decisions as to the accuracy required in the output to meet the educational needs (for instance accepting that secondary radiation would not be implemented in this version).

Future developments on the simulator will focus on expanding the range of teaching points addressed. For example, focal spot unsharpness and scattered radiation, thereby extending the capabilities of the simulators to support these points and conducting an in-depth student evaluation of the software in different teaching scenarios. Future developments could also allow EX-RayImage to be used in a wider educational context, such as image registration and surgical/interventional radiology training or planning. More in depth evaluation of the educational impact of the simulators is also important, investigating a the impact on a wider set of learning

points, more diverse students groups, and investigate how the tools might help students link theory and practice.

## **5 CONCLUSION**

We have developed two computer simulation environments for the delivery of physics education in radiological science in a practical and engaging way. This new innovative method of delivery provides an opportunity for experiential learning to a wide range of radiography, radiology and medical physics students across our institution. Our approach has enabled students to develop an understanding of the physical principles that are applied to practical situations without the need to access the clinical environment at this stage in their education.

## **REFERENCES**

- [1] M. Abdellah, A. Eldeib, M.I. Owis, GPU acceleration for digitally reconstructed radiographs using bindless texture objects and CUDA/OpenGL interoperability, Proc. Annu. Int. Conf. IEEE Eng. Med. Biol. Soc. EMBS. 2015-Novem (2015) 4242–4245. doi:10.1109/EMBC.2015.7319331.
- [2] M. Abdellah, M. Abdallah, M. Alzanati, A. Eldeib, Efficient Rendering of Digitally Reconstructed Radiographs on Heterogeneous Computing Architectures using Central Slice Theorem Mohamed, (2016) 3957–3960.
- [3] M. Abdellah, A. Abdelaziz, Parallel Generation of Digitally Reconstructed Radiographs on Heterogeneous Multi-GPU Workstations, (2016) 3953–3956.
- [4] A. Badal, A. Badano, Monte Carlo simulation of x-ray imaging using a graphics processing unit, 2009 IEEE Nucl. Sci. Symp. Conf. Rec. (2009) 4081–4084. doi:10.1109/NSSMIC.2009.5402382.

- [5] O.M. Dorgham, S.D. Laycock, M.H. Fisher, GPU accelerated generation of digitally reconstructed radiographs for 2-D/3-D image registration, *IEEE Trans. Biomed. Eng.* 59 (2012) 2594–2603. doi:10.1109/TBME.2012.2207898.
- [6] X. Jia, H. Yan, L. Cervino, M. Folkerts, S.B. Jiang, A GPU tool for efficient, accurate, and realistic simulation of cone beam CT projections., *Med. Phys.* 39 (2012) 7368–78. doi:10.1118/1.4766436.
- [7] D. Staub, M.J. Murphy, A digitally reconstructed radiograph algorithm calculated from first principles., *Med. Phys.* 40 (2013) 011902. doi:10.1118/1.4769413.
- [8] I.Y. Son, M. Winslow, B. Yazici, X.G. Xu, x-ray imaging optimization using virtual phantoms and computerized observer modelling., *Phys. Med. Biol.* 51 (2006) 4289–4310. doi:10.1088/0031-9155/51/17/011.
- [9] M. Winslow, X.G. Xu, B. Yazici, Development of a simulator for radiographic image optimization., *Comput. Methods Programs Biomed.* 78 (2005) 179–90. doi:10.1016/j.cmpb.2005.02.004.
- [10] S.C.A. Correa, E.M. Souza, A.X. Silva, D.H. Cassiano, R.T. Lopes, Computed radiography simulation using the Monte Carlo code MCNPX., *Appl. Radiat. Isot.* 68 (2010) 1662–1670. doi:10.1016/j.apradiso.2010.02.011.
- [11] D. Lazos, K. Bliznakova, Z. Kolitsi, N. Pallikarakis, An integrated research tool for x-ray imaging simulation., *Comput. Methods Programs Biomed.* 70 (2003) 241–51. <http://www.ncbi.nlm.nih.gov/pubmed/12581556>.
- [12] A. Sossin, J. Tabary, V. Rebuffel, J.M. Létang, N. Freud, L. Verger, Fast scattering simulation tool for multi-energy x-ray imaging, *Nucl. Instruments*

- Methods Phys. Res. Sect. A Accel. Spectrometers, Detect. Assoc. Equip. 802 (2015) 60–66. doi:10.1016/j.nima.2015.08.073.
- [13] J. Tabary, R. Guillemaud, F. Mathy, A. Glière, P. Hugonnard, Combination of high resolution analytically computed uncollided flux images with low resolution Monte Carlo computed scattered flux images, *IEEE Trans. Nucl. Sci.* 51 (2004) 212–217. doi:10.1109/TNS.2003.823038.
- [14] E. Gallio, O. Rampado, E. Gianaria, S.D. Bianchi, R. Ropolo, A GPU simulation tool for training and optimisation in 2D digital x-ray imaging, *PLoS One.* 10 (2015) 1–17. doi:10.1371/journal.pone.0141497.
- [15] A. Bernardini, V. Fanti, R. Marzeddu, G. Massazza, P. Randaccio, A Simulation Tool for X-Ray Imaging Systems, 00 (2004) 5–8.
- [16] V. Fanti, R. Marzeddu, G. Massazza, P. Randaccio, A simulation tool to support teaching and learning the operation of x-ray imaging systems, *Med. Eng. Phys.* 27 (2005) 555–559. doi:10.1016/j.medengphy.2004.11.010.
- [17] C.S. Moore, G.P. Liney, A.W. Beavis, J.R. Saunderson, A method to produce and validate a digitally reconstructed radiograph-based computer simulation for optimisation of chest radiographs acquired with a computed radiography imaging system, *Br. J. Radiol.* 84 (2011) 890–902. doi:10.1259/bjr/30125639.
- [18] S.K. Ahn, G. Cho, Y.K. Chi, H.K. Kim, M. Jae, A computer code for the simulation of x-ray imaging systems, 2003 IEEE Nucl. Sci. Symp. Conf. Rec. (IEEE Cat. No.03CH37515). 2 (2003) 838–842. doi:10.1109/NSSMIC.2003.1351828.
- [19] A. Dikshit, D. Wu, C. Wu, W. Zhao, An online interactive simulation system for

- medical imaging education, *Comput. Med. Imaging Graph.* 29 (2005) 395–404.  
doi:10.1016/j.compmedimag.2005.02.001.
- [20] P. Duvauchelle, N. Freud, V. Kaftandjian, D. Babot, A computer code to simulate x-ray imaging techniques, *Nucl. Instruments Methods Phys. Res. Sect. B Beam Interact. with Mater. Atoms.* 170 (2000) 245–258.  
doi:10.1016/S0168-583X(00)00185-3.
- [21] N. Freud, P. Duvauchelle, J.M. Létang, D. Babot, Fast and robust ray casting algorithms for virtual x-ray imaging, *Nucl. Instruments Methods Phys. Res. Sect. B Beam Interact. with Mater. Atoms.* 248 (2006) 175–180.  
doi:10.1016/j.nimb.2006.03.009.
- [22] N. Freud, P. Duvauchelle, D. Babot, New developments in virtual x-ray imaging: Fast simulation using a deterministic approach, *AIP Conf. ....* 22 (2003) 553–560. [https://extras.springer.com/2003/978-0-7354-0117-4/cdr\\_pdfs/indexed/553\\_1.pdf](https://extras.springer.com/2003/978-0-7354-0117-4/cdr_pdfs/indexed/553_1.pdf).
- [23] MATLAB, 2014. Version 8.3.0.532 (R2014a), (n.d.).
- [24] K. Cranley, B. Gilmore, G. Fogarty, L. Desponds, Catalogue of diagnostic x-ray spectra and other data. IPEM Report 78 (CD-ROM), 1997.
- [25] J.H. Hubbell, S.M. Seltzer, Tables of x-ray mass attenuation coefficients and mass energy-absorption coefficients (version 1.4). [Online], (2004).  
<http://physics.nist.gov/xaamdi> (accessed July 20, 2016).
- [26] N. Mitsuhashi, K. Fujieda, T. Tamura, S. Kawamoto, T. Takagi, K. Okubo, BodyParts3D: 3D structure database for anatomical concepts, *Nucleic Acids Res.* 37 (2009). doi:10.1093/nar/gkn613.

[27] T. Moller, B. Trumbore, Fast, minimum storage ray-triangle intersection, J. Graph. Tools. 2 (1997) 21–28.

## FIGURE LEGENDS

Figure 1. System Design Overview

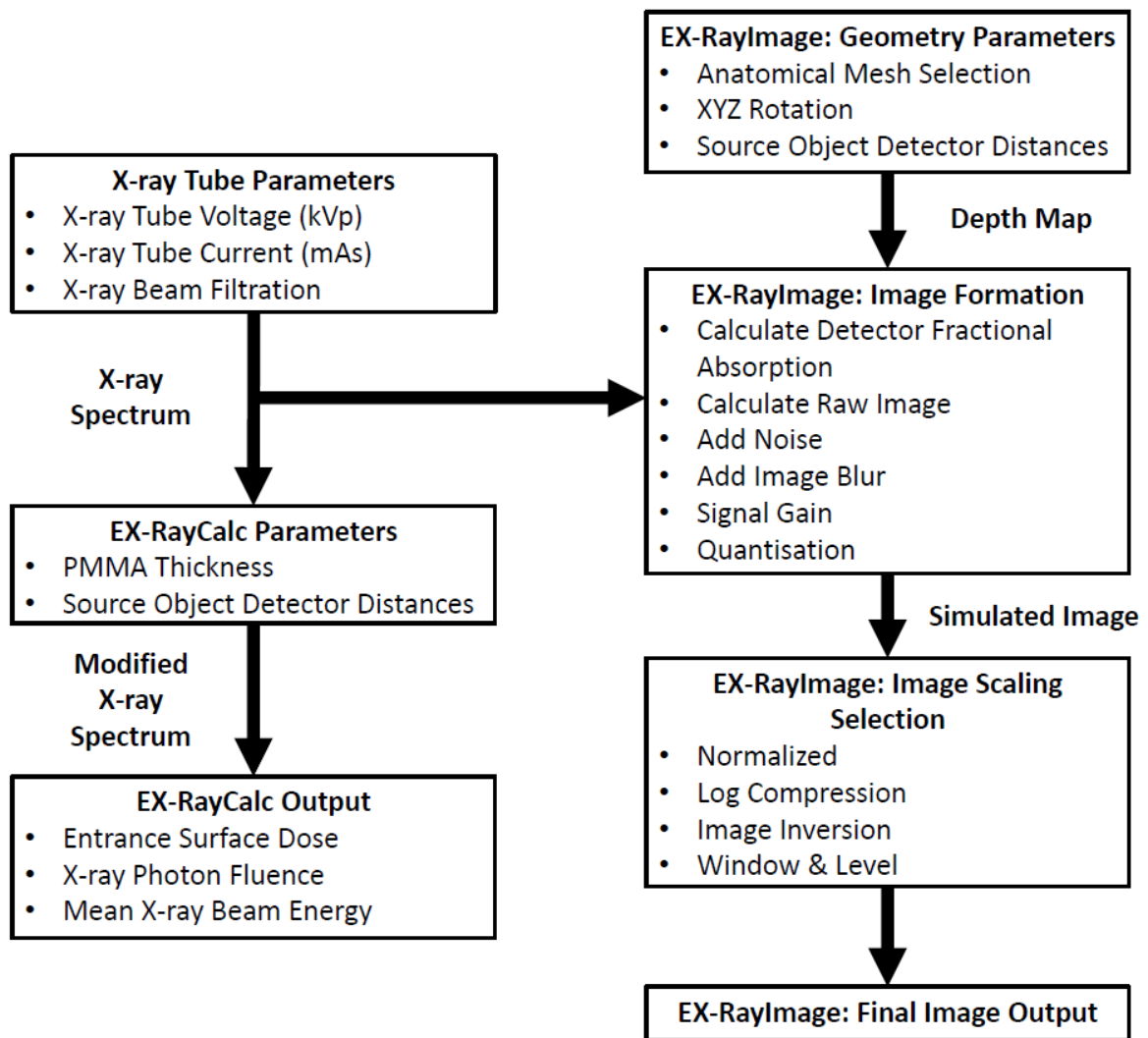


Figure 2. Experimental setup

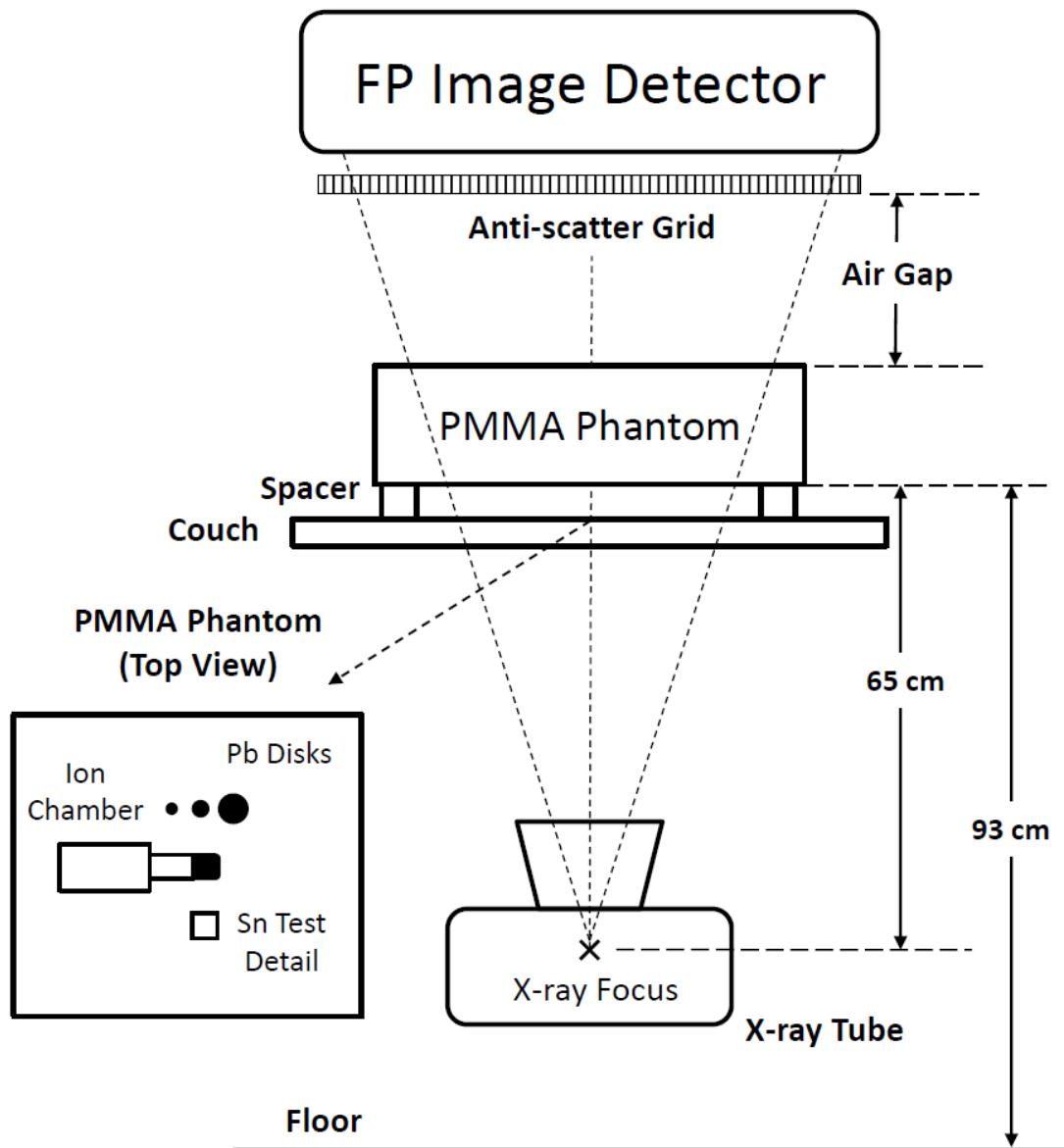


Figure 3. Position of point P on a plane

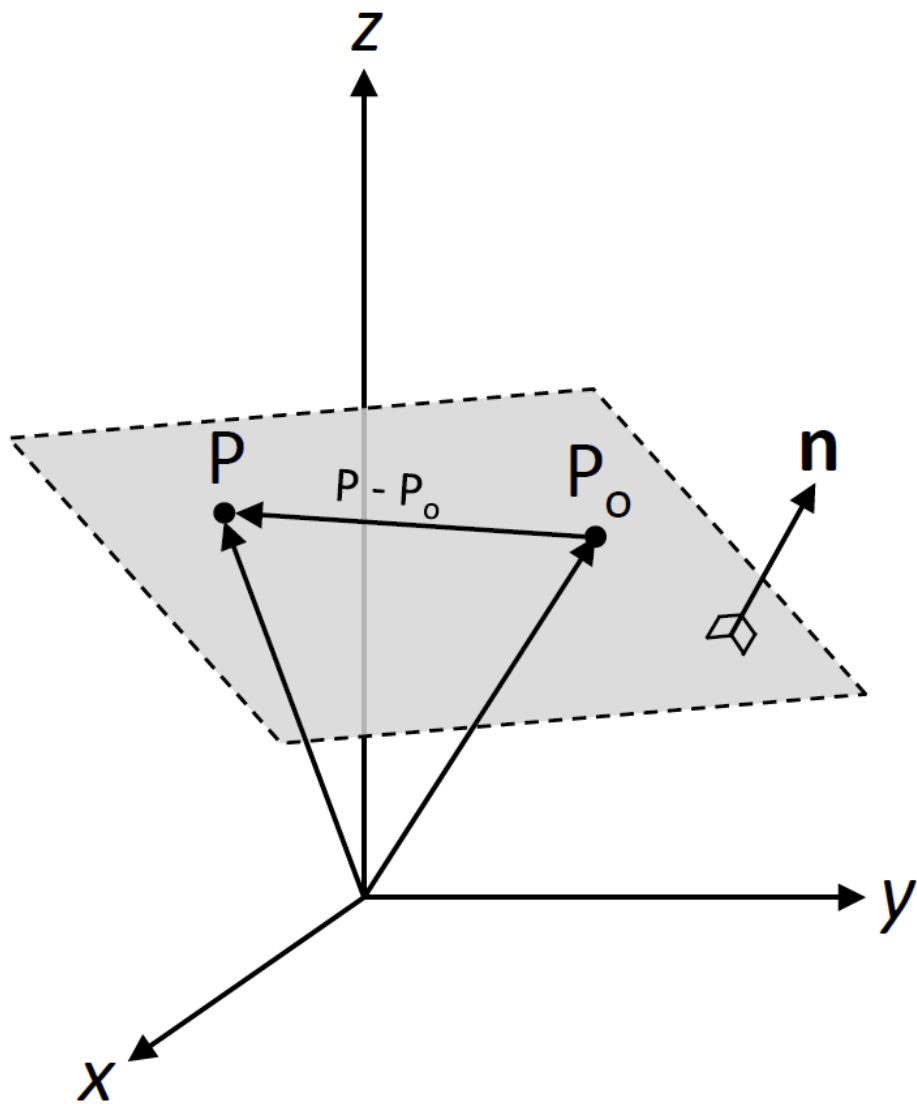


Figure 4. Forward projection of mesh face onto detector plane

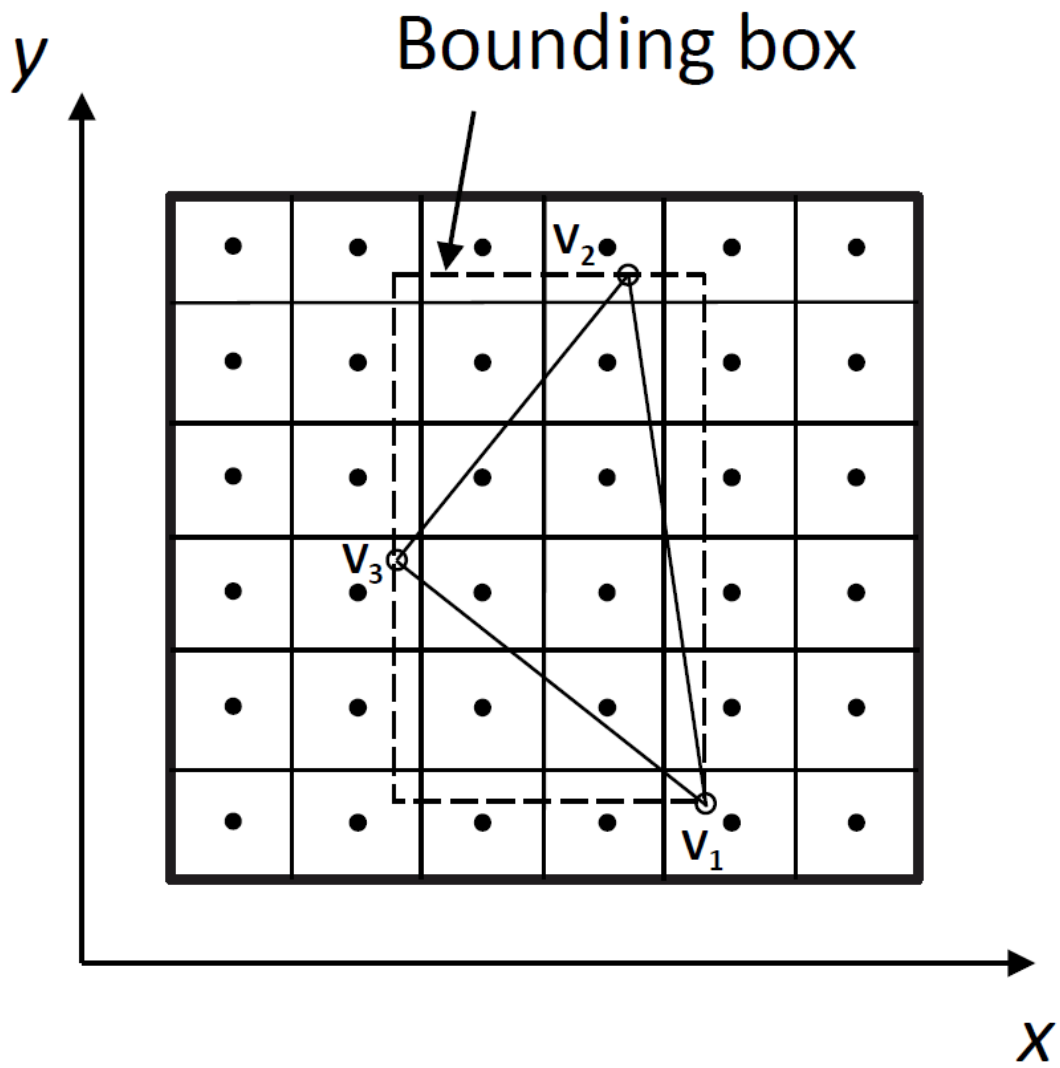


Figure 5. Multi-mesh cases tracked by algorithm (M – mesh, T - material represented)

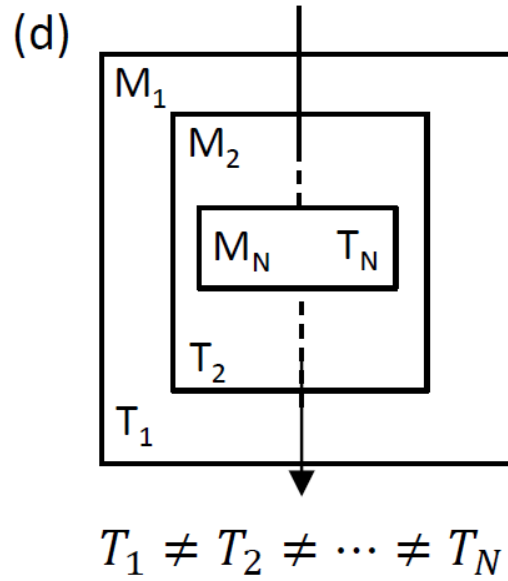
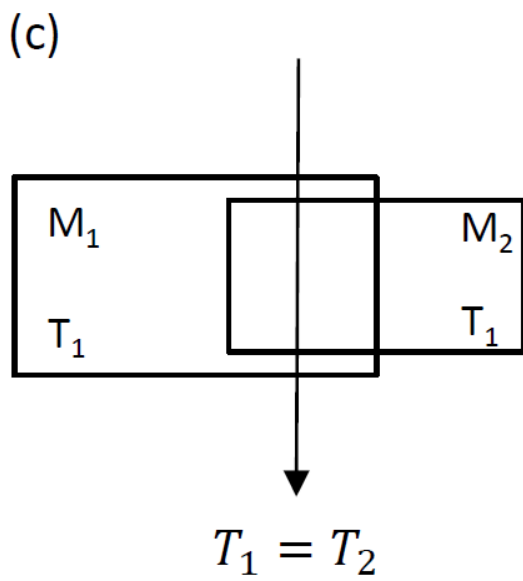
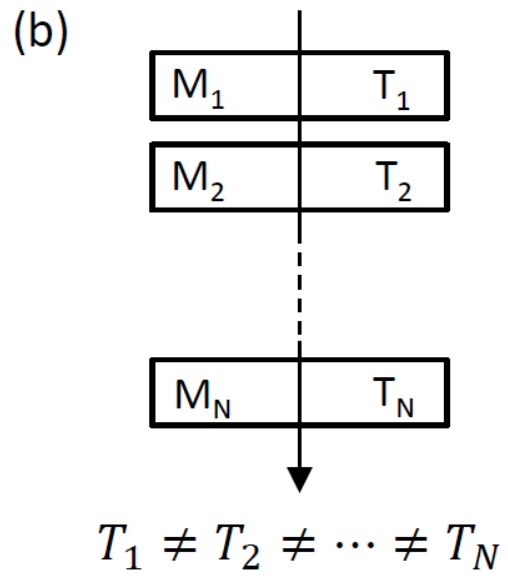
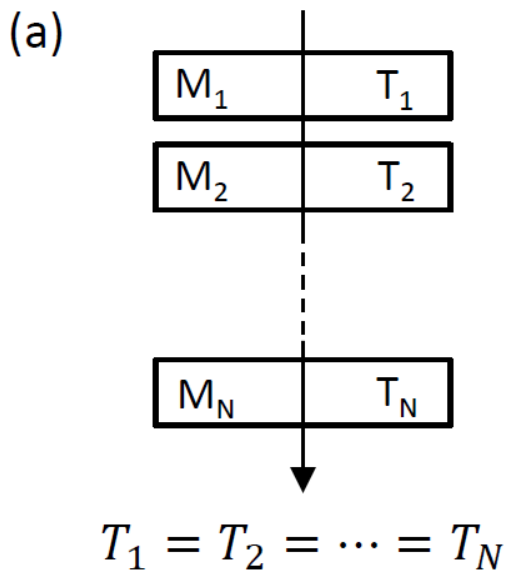


Figure 6. EX-RayCalc graphical user interface

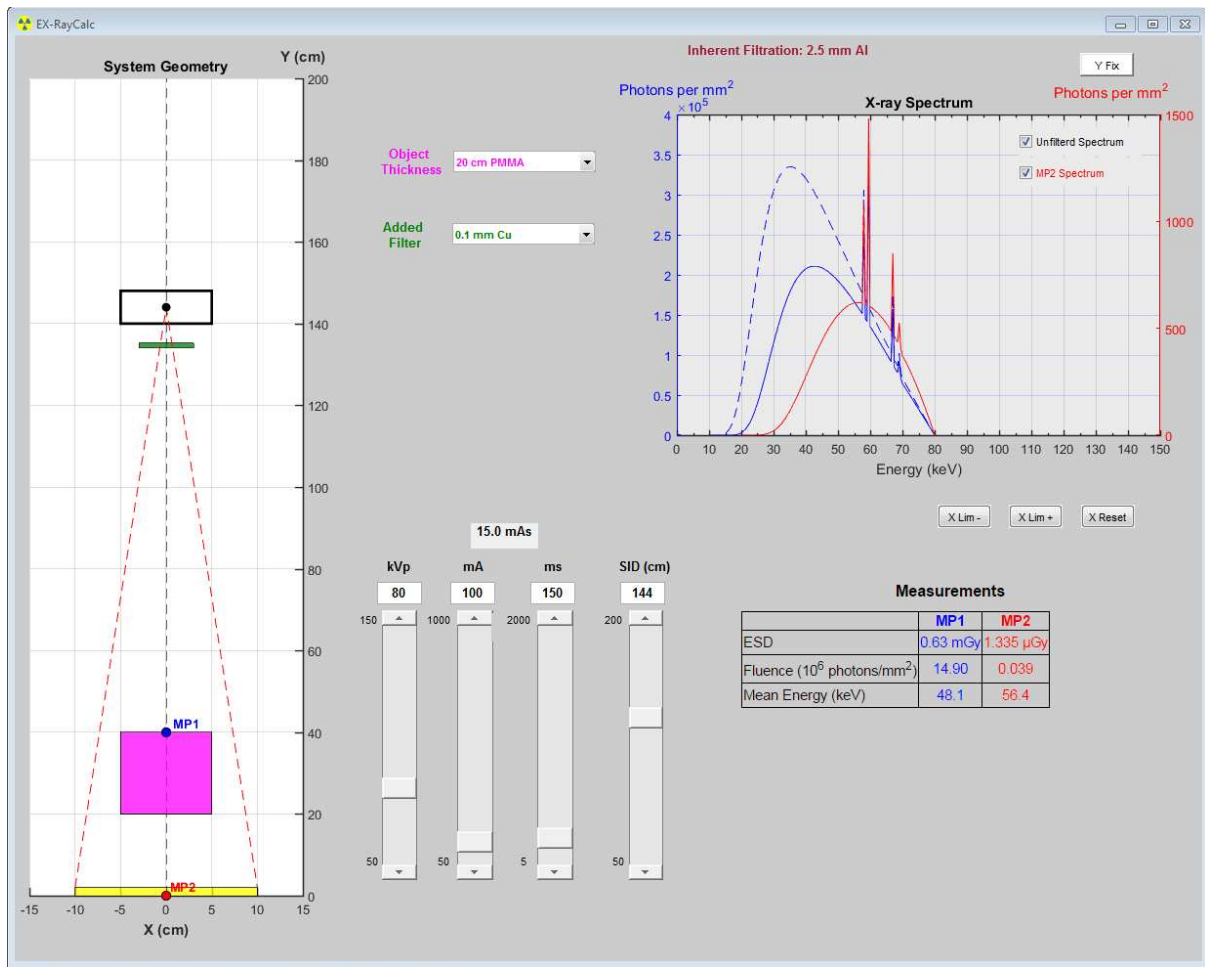


Figure 7. EX-RayCalc validation results

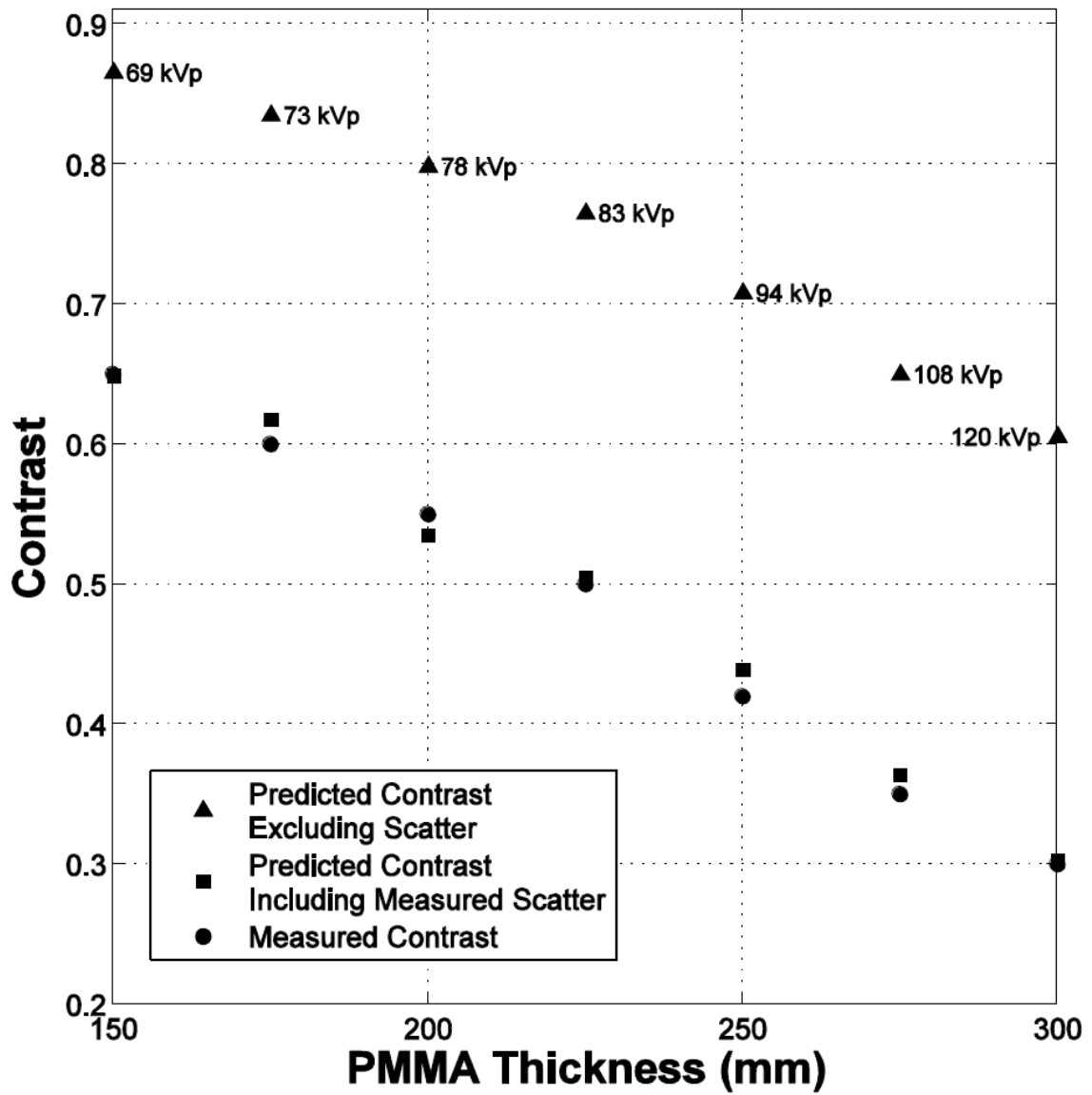
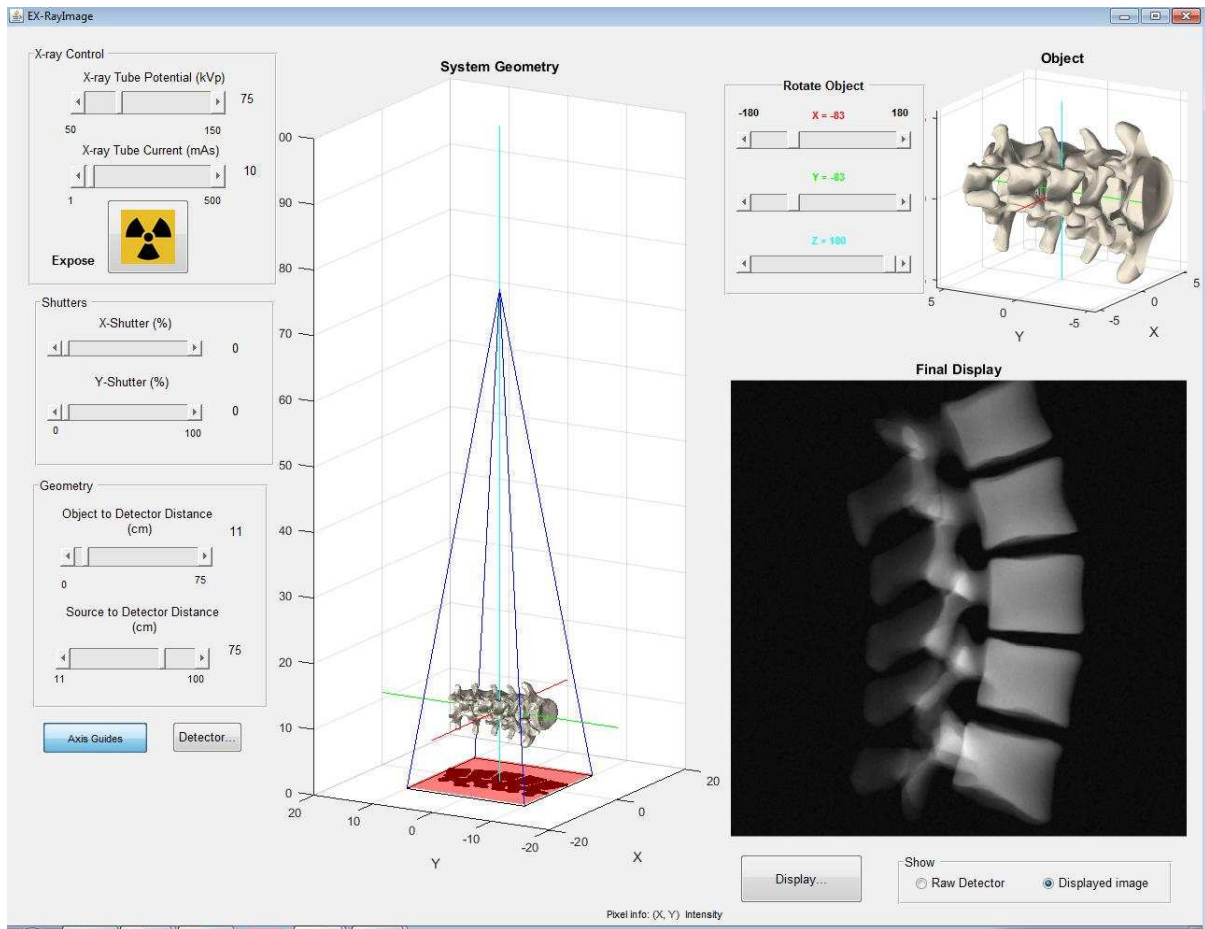
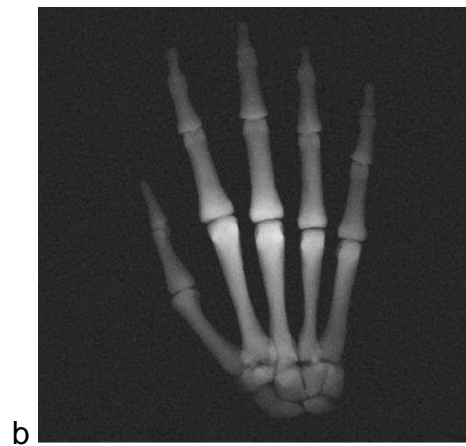
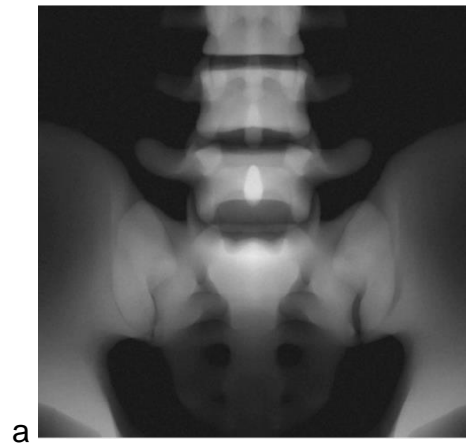


Figure 8. EX-RayImage graphical user interface



**Figure 9. Multiple anatomical areas simulated with the EX-RayImage: a) pelvis, b) hand/wrist and c) elbow.**



**Figure 10 Two simulated radiographs generated with different exposure conditions**

